



## OPEN

## SUBJECT AREAS:

BIOMEDICAL  
ENGINEERING

NANOPARTICLES

DRUG DELIVERY

TRANSFECTION

Received

12 August 2013

Accepted

17 October 2013

Published

6 November 2013

Correspondence and  
requests for materials  
should be addressed to  
K.W.L. (kam.leong@  
duke.edu)

# Microfluidic Preparation of Polymer-Nucleic Acid Nanocomplexes Improves Nonviral Gene Transfer

Christopher L. Grigsby<sup>1</sup>, Yi-Ping Ho<sup>2</sup>, Chao Lin<sup>3</sup>, Johan F. J. Engbersen<sup>4</sup> & Kam W. Leong<sup>1,5</sup><sup>1</sup>Department of Biomedical Engineering, Duke University, 136 Hudson Hall, Box 90281, Durham, NC 27708, USA,<sup>2</sup>Interdisciplinary Nanoscience Center (iNANO), Aarhus University, Gustav Wieds Vej 14, DK-8000 Aarhus C, Denmark, <sup>3</sup>Institute for Biomedical Engineering and Nanoscience, Tongji University School of Medicine, Tongji University, 200092, Shanghai, PR China, <sup>4</sup>Department of Biomedical Chemistry, MIRA Institute for Biomedical Technology and Technical Medicine, University of Twente, P.O. Box 217, 7500 AE Enschede, The Netherlands, <sup>5</sup>Center of Excellence for Advanced Materials Research, King Abdulaziz University, Jeddah 21589, Saudi Arabia.

As the designs of polymer systems used to deliver nucleic acids continue to evolve, it is becoming increasingly apparent that the basic bulk manufacturing techniques of the past will be insufficient to produce polymer-nucleic acid nanocomplexes that possess the uniformity, stability, and potency required for their successful clinical translation and widespread commercialization. Traditional bulk-prepared products are often physicochemically heterogeneous and may vary significantly from one batch to the next. Here we show that preparation of bioreducible nanocomplexes with an emulsion-based droplet microfluidic system produces significantly improved nanoparticles that are up to fifty percent smaller, more uniform, and are less prone to aggregation. The intracellular integrity of nanocomplexes prepared with this microfluidic method is significantly prolonged, as detected using a high-throughput flow cytometric quantum dot Förster resonance energy transfer nanosensor system. These physical attributes conspire to consistently enhance the delivery of both plasmid DNA and messenger RNA payloads in stem cells, primary cells, and human cell lines. Innovation in processing is necessary to move the field toward the broader clinical implementation of safe and effective nonviral nucleic acid therapeutics, and preparation with droplet microfluidics represents a step forward in addressing the critical barrier of robust and reproducible nanocomplex production.

As the range of known potential targets for therapeutic molecular intervention expands, nucleic acid-based drugs are poised to play a more prominent role in the treatment of inherited and acquired human diseases. Recent clinical trials hint at the therapeutic potential of gene therapy, but this potential remains stymied by the dearth of safe and efficient delivery systems<sup>1–4</sup>. One approach has been to use cationic polymers to condense nucleic acids into nanocomplexes (polyplexes) that facilitate cellular uptake and prevent degradation *en route* to target cells. While tremendous creativity and innovation in carrier design have produced very sophisticated polymeric gene delivery systems, nonviral methods remain prohibitively inefficient for most applications<sup>5–9</sup>. The circulatory residence time, cellular uptake, transfection efficiency, and toxicity of nanoparticles all depend to some extent on physicochemical attributes such as size, stability, shape, and charge<sup>10,11</sup>. However, the physical aspects of polyplex production, and their role in determining these properties, have been largely overlooked.

The assembly of nanocomplexes by charge neutralization is a process that occurs in milliseconds<sup>12,13</sup>. While preparation in bulk formats by pipetting, shaking, or oscillatory mixing is convenient, these methods are poorly suited to reproducibly generate uniform particles given the kinetically determined nature of the formation process<sup>14</sup>. Irreproducibility is typical; slight perturbations of bulk mixing protocols often yield particles of varied properties. The poor quality of these polyplexes exacerbates the challenge of establishing precise structure-function relationships and precludes mechanistic understandings of the gene transfer process, as subpopulations of particles may be responsible for observed phenomena. The inability to manufacture nonviral delivery systems in a reproducible and scalable manner also hinders their clinical translation. As the field has begun to consider the physical control of nanoparticle assembly as an opportunity for innovation, several novel techniques have emerged<sup>15–17</sup>. Top-down nanoimprinting systems produce nanoparticles with defined shape and size that have proven valuable in deconvoluting the mechanistic effects of such characteristics. However, the rapid reaction kinetics, aqueous conditions, and temperature sensitivity of polyplex assembly favor microfluidic approaches,



which have included both monophasic laminar flow systems and emulsion-based designs<sup>13,18–22</sup>. The former suffer from flocculation at high concentrations, while the latter have been used successfully in production of both lipoplexes and polyplexes. Here, we have used an emulsion-based microfluidic system to confine the synthesis of polyplexes to picoliter sized water-in-oil droplets. This system for microfluidics assisted confinement (MAC) enables the mixing of polyelectrolyte components to proceed more rapidly so that polyplexes are formed under equilibrium conditions.

For such a system to be broadly useful, it must perform well with different payloads and across multiple cell types. Plasmid DNA is the predominant payload in gene delivery, but messenger RNA eliminates the requirement of nuclear delivery and more easily produces transgene expression in some slowly dividing or post-mitotic cells. However, substitution of the payload may not be trivial, as there is mounting evidence that polycations interact differently with DNA than they do with RNA<sup>23</sup>. Double stranded DNA is a stiffer molecule with a longer persistence length than single-stranded messenger RNA, and shorter nucleic acids may diminish the effects of molecular chain entanglement. In line with our aim to establish the broad potential of MAC to control polyplex self-assembly, in this study we utilized a promising bioreducible linear poly(amido amine) gene carrier and hypothesized that DNA polyplexes prepared with MAC would be more homogeneous and more potent. Next, we tested whether the benefits of MAC preparation would also apply to complexes loaded with RNA payloads and probed their potency in multiple translationally relevant and difficult-to-transfect target cell types. We evaluated the products in terms of size, polydispersity, zeta potential, binding stability, aggregation behavior, amount of unreacted polyanion species, and transfection efficiency. Through the use of a quantum dot Förster resonance energy transfer (QD-FRET) based assay, we furthermore quantified the cellular uptake and intracellular unpacking of MAC polyplexes in an attempt to correlate their performance with their ability to overcome these two specific rate-limiting barriers to delivery. This study helps bridge a void in the structure-function understanding of gene delivery by demonstrating how physical polyplex attributes dictated by their preparation can influence intracellular behavior and transfection efficiency. Together, the results of these studies demonstrate that nonviral gene delivery can be improved not only by chemical design and optimization, but also through innovation in processing and preparation techniques.

## Results

**Polyplex preparation and physical characterization.** We prepared polyplexes loaded with either plasmid DNA or messenger RNA using the bioreducible linear poly(amido amine) poly(CBA-ABOL) in bulk and MAC formats (Figure 1). We selected this gene carrier for its high efficiency, low toxicity, and ability to deliver multiple types of nucleic acids<sup>24,25</sup>. Following a systematic optimization of binding characteristics, DNA and RNA polyplexes were synthesized exclusively at polymer:nucleic acid mass ratios of 45:1 and 60:1, respectively (Supplementary Figure 1). In both cases, preparation with MAC resulted in the production of smaller and more monodispersed polyplexes. The Z-average diameters of MAC polyplexes were 40–50% smaller than those of bulk controls immediately following synthesis (Figure 2A). The width of the size distribution was also significantly reduced, as evidenced by similar reductions in the polydispersity index (PDI). To quantify the propensity of the products to aggregate, we additionally measured changes in polyplex size at five-minute intervals over the course of a typical four-hour transfection period (Figure 2B). Bulk polyplexes began to aggregate immediately, and continued to grow in size throughout the period studied. In contrast, MAC polyplexes exhibited a much higher degree of colloidal stability and remained approximately unchanged in size throughout the measurement period. The surface charge density of the polyplexes, represented by the zeta-potential, was also considered (Figure 2C). MAC polyplexes exhibited lower zeta-potentials, suggesting more complete charge neutralization or the presence of a diminished polymer corona, either of which may contribute to improved colloidal stability by reducing charge imbalances and intraparticle heterogeneity<sup>26</sup>. The physical profiles of nanoparticles are important, as the putative rate-limiting barriers associated with the low efficiency of nonviral vectors include cellular binding and uptake, endosomal escape, cytosolic transport and unpacking, nuclear entry, and transcriptional processing. Physical particle properties determine the degree to which particles are able to overcome each of these hurdles. Knowing that MAC preparation yields smaller, more monodispersed, and less positively charged DNA and RNA polyplexes, we next examined complex binding stability and the final disposition of the polymer component following the complexation reaction.

**Analysis of complexation and binding.** A common shortcoming of bulk preparation is the failure to exhaust the molecular reactants

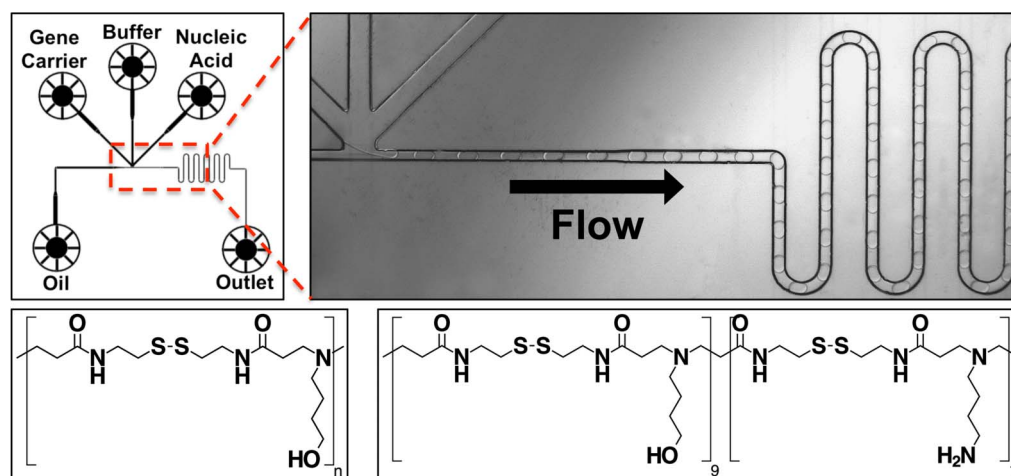


**Figure 1** | Design of microfluidic chip and gene carriers. (A) A microfluidic cross-flow droplet generator chip is used to produce emulsified aqueous droplets containing the polymeric gene carrier and nucleic acids. While confined to these  $\sim 100$  pL droplets, the polyions self-assemble into nanocomplexes. Following collection and disruption of the droplets, the polyplexes are collected and used directly. Channel dimensions are  $50 \mu\text{m}$  (width)  $\times 35 \mu\text{m}$  (height) (B) Chemical structure of p(CBA-ABOL) (C) Chemical structure of p(CBA-ABOL90/BDA10).

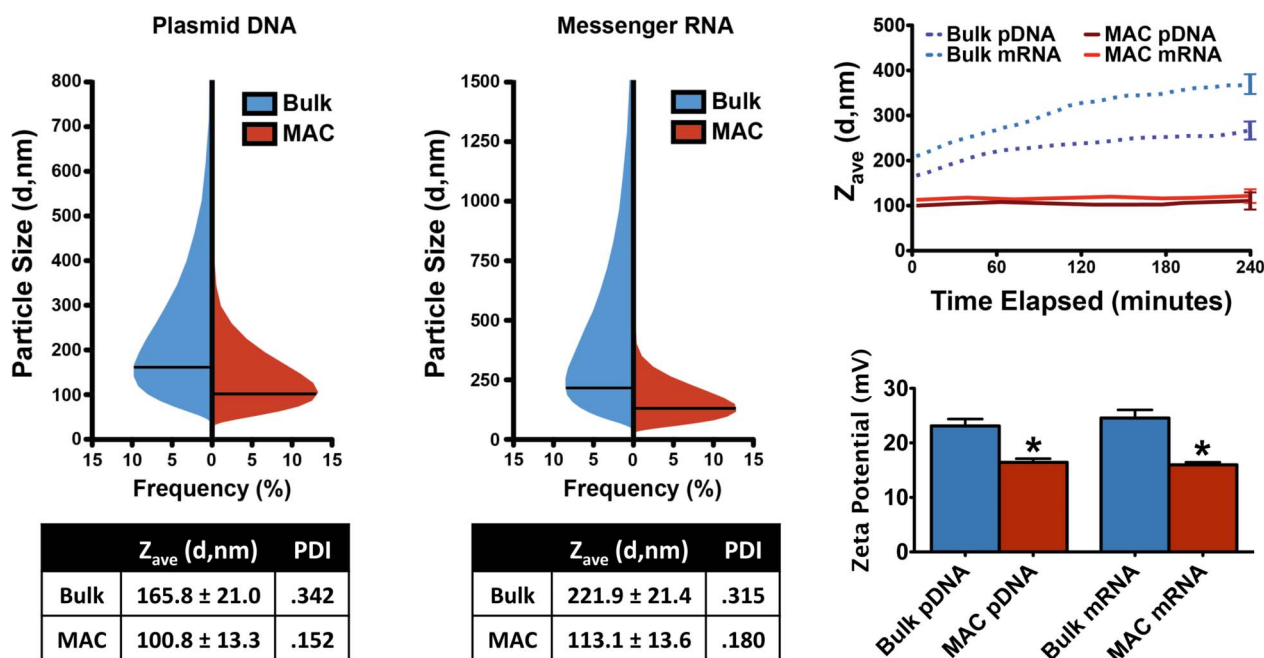


**Figure 2** | Size and charge characterization of nanocomplexes. (A) Size frequency distributions by intensity of polyplexes measured by dynamic light scattering immediately following preparation, with  $Z$ -average diameters indicated with black lines.  $Z$ -average diameter  $\pm$  SEM and polydispersity indices are reported below for bulk and MAC preparations of both pDNA and mRNA polyplexes ( $n = 5$  each). (B) Aggregation propensity shown as the  $Z$ -average diameter over time ( $n = 5$  each, measured at 5 minute intervals) (C) Zeta potential for each type of polyplex, shown as mean  $\pm$  SEM and analyzed with student's  $t$ -test (\*  $p < 0.05$ ) ( $n = 5$  each).

due to the rapid complexation under chaotic and heterogeneous conditions. This is problematic because excess unreacted polymer has been shown to contribute to polyplex aggregation and cytotoxicity during transfection<sup>27</sup>. To quantify the amount of unreacted polymer left in solution, we prepared 10  $\mu$ g nucleic acid doses of polyplexes with p(CBA-ABOL) and Cy5-labeled p(CBA-ABOL90/BDA10) in a 4:1 ratio. Following preparation, we removed the polyplexes by centrifugation. The supernatant was lyophilized, reconstituted in 100  $\mu$ L complexation buffer, and transferred to a 96-well plate for quantification of the remaining excess polymer. MAC preparation significantly reduced the fraction of polymer left unreacted (Figure 3A). To further probe the composition of MAC polyplexes, we then measured the binding stability between polymer and payload using a fluorescence-based binding assay. PicoGreen and RiboGreen are cationic dyes that fluoresce upon intercalation with DNA or RNA, respectively. When added in increasing concentrations to intact polyplexes, they compete with the gene carrier to bind nucleic acids. As complexes are disrupted by the

competition and the shielding of the nucleic acids by the polymer is diminished, the fluorescent signal of the dye intensifies accordingly with little background signal from unbound reagent. Consequently, the increase in fluorescence indicates the level of decomplexation between nucleic acid and polymer. As seen in Figure 3B and 3C, the MAC polyplexes remained comparatively more intact as increasing concentrations of competitor were introduced. At the maximum competitor concentrations, bulk controls were significantly disrupted while MAC polyplexes remained resistant. Such increased binding stability and resistance to competitive disruption may lead to better protection from premature degradation and a more sustained intracellular release of payload. However, this relationship depends on the gene carrier involved; some polymers bind nucleic acids too tightly to efficiently deliver them to the nucleus<sup>28</sup>. While this is less likely to occur with bioreducible and biodegradable carriers such as the one used here, further analysis was necessary to demonstrate that increased complexation and tighter binding leads to improved activity.

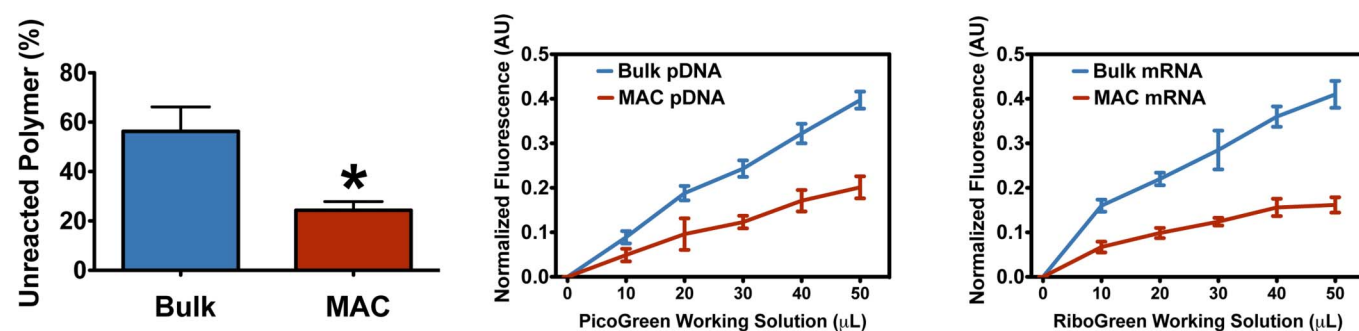


**Figure 3** | Unreacted polymer and binding stability of nanocomplexes. (A) The amount of unreacted Cy5-labeled polymer remaining in the product from each method was quantified after removal of pDNA polyplexes by centrifugation. (B), (C) Binding stabilities of pDNA and mRNA polyplexes were measured using PicoGreen and RiboGreen competition assays, respectively. Fluorescence was corrected for background signal and normalized such that polymer-free controls = 1.0 arbitrary units (AU). Data is shown as mean  $\pm$  SEM ( $n = 3$  each).



**Transfection efficiency and cellular uptake.** The most critical aspect of polyplex performance is transfection efficiency. We tested both DNA and RNA polyplexes in four cell types that spanned the most common target classes for gene delivery applications. Primary mouse embryonic fibroblast (PMEF) cells were selected for their prevalence in the cellular reprogramming and induced pluripotent stem cell fields. Human mesenchymal stem cells (hMSC) were included to represent primary human adult stem cells. HepG2 human hepatocellular carcinoma cells were tested due to their characteristic low transfectability and the importance of hepatocytes as a destination for gene delivery systems designed to target the liver. Lastly, HEK293 human embryonic kidney cells were chosen to compare with the large body of prior work. At 24 hours following delivery to the four different cell types, the transfection efficiency polyplexes loaded with 1  $\mu\text{g}$  pDNA or mRNA encoding GFP was assessed with fluorescence microscopy and quantified by flow cytometry. In each case, transfection with MAC polyplexes resulted in a larger fraction of cells expressing the GFP reporter protein (Figure 4A and 4B). The gains ranged from 6 to 31 percent more cells transfected, and were particularly significant in difficult-to-transfect cell types such as HepG2 and hMSC. Several different doses of polyplexes were delivered to HEK293 cells to verify that this result was not dose-dependent, and the improvement persisted across the range of doses (Figure 4C). In some applications, the total level of transgene produced may be more important than the number of individual cells transfected. To measure gross transgene expression, 1  $\mu\text{g}$  doses of pDNA encoding luciferase was delivered to each of the four cell types. In each case, transfection with MAC polyplexes resulted in 1.9 to 6.8-fold higher total expression as quantified by luminescence detection (Figure 4D). Cytotoxicity comparisons are not

shown, as poly(CBA-ABOL) is effectively non-toxic at single dose levels (Supplementary Figure 3).

To elucidate the mechanistic relationship between the physical attributes of MAC polyplexes and their improved performance, we focused on two of the primary rate-limiting barriers of nonviral gene delivery: cellular uptake and intracellular unpacking. Although the optimal dimensions of particles for cellular uptake remain a topic of debate, endocytosis is believed to be a size-dependent process<sup>29</sup>. It follows that the most straightforward means for MAC to improve transfection would be through an increase in cellular uptake due to the smaller size of MAC polyplexes. We measured cellular uptake in a high-throughput manner using flow cytometric detection of internalized QD-labeled pDNA. Bulk and MAC polyplexes were delivered to HEK293 cells, which were fixed to arrest endocytosis at defined timepoints and washed with heparin to remove any remaining membrane-associated complexes. Flow cytometry was used to detect the percentage of cells containing the labeled plasmid at each point, as well as the mean fluorescence signal that correlates with the total mass of internalized plasmid. We observed no difference in uptake between bulk and MAC prepared polyplexes over the time course of a typical transfection period by either metric (Figure 5B and 5C). While the size of MAC polyplexes is reduced, the difference may not be sufficient to alter the rates or modes of endocytosis. If increased uptake is not responsible for the functional benefits of MAC polyplexes, the improvements likely arise from a subsequent process.

**Intracellular behavior of nanocomplexes.** Next, we used QD-FRET detection to examine the intracellular decondensation rates of MAC polyplexes. Förster resonance energy transfer (FRET) is a technique

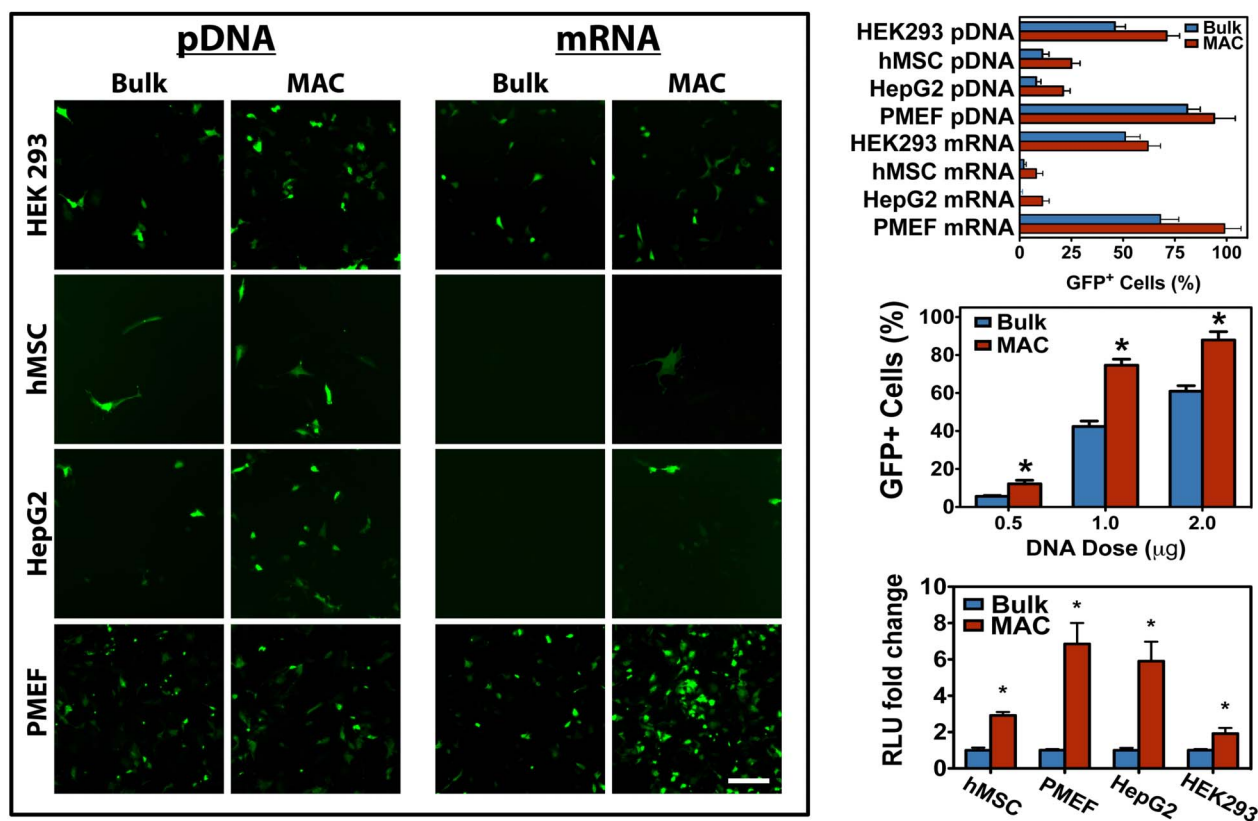


**Figure 4 | Transfection efficiency in four cell types.** (A) Fluorescence micrographs of four cell types transfected with bulk or MAC polyplexes loaded with 1  $\mu\text{g}$  of either pDNA or mRNA encoding GFP. Scale bar = 50  $\mu\text{m}$  (B) Quantification of GFP transfection efficiency with flow cytometry ( $p < 0.05$  in each case) (C) Transfection efficiency in HEK293 cells across a range of doses confirms that the increased transfection by MAC polyplexes is not dose-dependent. (D) Quantification of total transgene expression following transfection with pLuc DNA complexes.

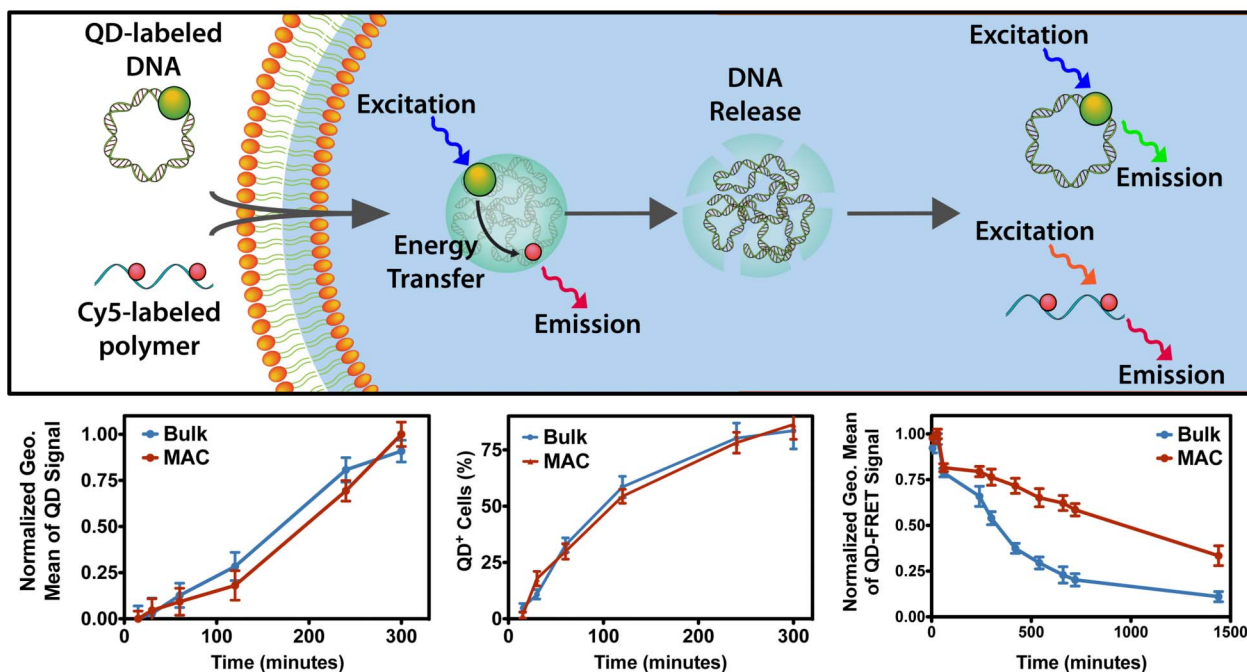


**Figure 5 | Cellular internalization and intracellular unpacking.** (A) Labeling scheme to detect uptake and unpacking using QD-FRET. Biotinylated pDNA was labeled with QD energy donors, while the polymer was functionalized with the Cy5 QD-FRET acceptor. QD-FRET emission is detected while polyplexes are intact. Following unpacking, QD-FRET signal is lost and separate donor and acceptor emissions are recovered. (B), (C) Cellular internalization was quantified by measuring the fluorescence signal of QD-labeled pDNA in cells at different time points using flow cytometry. No significant difference was observed in the rates of uptake by cell number of normalized geometric mean fluorescence. (D) Intracellular unpacking was quantified by measuring the QD-FRET signal in cells at different time points using flow cytometry. Bulk controls unpacked more rapidly than MAC polyplexes ( $p < 0.05$  for all timepoints after 300 min).

that provides the unique ability to resolve molecular interactions beyond the diffraction limit of conventional microscopy. When FRET occurs, a donor fluorophore excites an acceptor via a nonradiative dipole–dipole interaction if they are sufficiently close (within  $\sim 10$  nm). This so-called ‘molecular ruler’ can be used to determine distances between labeled molecules inside cells, including gene carriers and nucleic acids<sup>30</sup>. Fluorescence colocalization methods do not offer the requisite sensitivity to precisely detect the onset of particle dissociation, to differentiate between molecules that are interacting or simply adjacent, or allow for high-throughput analysis. Furthermore, conventional fluorophores suffer from chemical and photodegradation, photobleaching and broad spectra. Conversely, semiconductor QDs possess broad absorption spectra, tunable narrow emission spectra, resistance to bleaching and chemical degradation, and large energy separation between excitation and emission eliminating the need for ratiometric disambiguation. In our case, excited QD donors transfer energy to Cy5 acceptors as long as polyplexes containing both constituents remain intact. When the complexes dissociate, the energy donors and acceptors become separated and the FRET-mediated Cy5 emission is lost, giving a precise digital indication of polyplex dissociation (Figure 5A). It has been previously shown that QD-FRET labeling does not significantly alter the physical properties or bioactivity of polyplexes<sup>28</sup>. We again chose flow cytometric detection to acquire precise temporal data on the intracellular unpacking rates. It was assumed that at the first time point, most of the polyplexes would still be intact, with FRET-mediated emission signal deteriorating over time as polyplexes unpacked. The values at the first point were thus chosen to represent maximum complexation. Over 24 hours following transfection, MAC polyplexes remained intact much longer than the more quickly unpacked bulk samples (Figure 5D). For example, by the six-hour time point, the QD-FRET signal for bulk polyplexes had decayed to less than half of its

maximum. Meanwhile, the MAC signal still exceeded 75 percent of its initial value. This prolonged intracellular stability may provide better payload protection prior to endosomal escape, as well as a more sustained release of the nucleic acid that may increase the chances of nucleic acids penetrating the nucleus during cell division. This flow cytometric population-level rate quantification shows that the increased extracellular stability of MAC polyplexes translates to the intracellular domain. This study therefore identifies a mechanistic relationship whereby controlling the physical assembly of nanocomplexes with MAC enables the modulation of polyplex properties to achieve improved nonviral gene transfer.

## Discussion

The development of safe and effective gene carriers is critical to the eventual success of nonviral gene therapy, and optimizing the assembly processes used to prepare polymer–nucleic acid nanocomplexes is one strategy to move toward this goal. We have reported the benefits of a microfluidic approach to better control the preparation of polyplexes and to produce more uniform and more potent delivery systems. While polymer–DNA nanocomplexes have been synthesized by microfluidics, to our knowledge this is the first example of the production of polymer–RNA nanocomplexes with a droplet-based microfluidic approach, as well as the first time that QD-FRET has been used in combination with flow cytometry to quantify the intracellular unpacking of polymer–DNA nanocomplexes. We have demonstrated that MAC polyplexes exhibit significant and consistent decreases in size, zeta potential, and polydispersity relative to complexes synthesized by traditional bulk mixing. Both DNA- and RNA-loaded nanocomplexes exhibit increased colloidal and binding stability, as quantified by fluorescence-based competitive binding assays. Transfection was significantly improved in a broad range of cell types, in terms of both the number of cells transfected and gross transgene expression. We ascribed this improvement in part to a



more gradual release of nucleic acids offered by MAC nanocomplexes, evidenced by the slower decline of intracellular QD-FRET emission. MAC preparation not only improves the biological performance of polyplexes, but may also help establish clearer structure-function relationships to guide future carrier design and advance nonviral gene therapy.

## Methods

**Polymer synthesis and labeling.** Poly(CBA-ABOL) was synthesized by Michael-type polyaddition of 3.67 g N,N-cystaminebisacrylamide (CBA) (Polysciences, Warrington, PA) and 1.26 g 4-amino-1-butanol (ABOL) (Sigma-Aldrich, Saint Louis, MO) as described by Lin *et al.*<sup>31</sup>. The reaction product was purified by dialysis (3.5 kDa cutoff) in acidic deionized water (pH 4) and then lyophilized. The polymer was collected in its HCl-salt form (1.63 g, 33% yield). Due to the absence of primary amines on poly(CBA-ABOL) for conjugation of fluorescent labels, we also synthesized the copolymer poly(CBA-ABOL90/BDA10) by substituting 10% N-Boc-1,4-butanediamine (BDA) for 4-amino-1-butanol in the polymerization. Deprotection of the Boc-protected amino groups in the copolymers was performed in a mixture of methanol/trifluoroacetic acid (10 mL, 1/1, v/v) overnight prior to dialysis. The primary amines on the BDA side chains of the copolymer were then functionalized with Cy5-NHS (Amersham Biosciences, Piscataway, NJ) fluorescent dye and purified again by dialysis. Labeled polymer was used in a 1:4 ratio with unlabeled p(CBA-ABOL) to maximize the efficiency of the QD-FRET sensor. The incorporation of fluorescent labels did not affect the size, zeta potential, or transfection efficiency of polyplexes. Both polymer structures were validated by Matrix Assisted Laser Desorption/Ionization (MALDI) mass spectrometry and <sup>1</sup>H NMR (not shown).

**Nucleic acid production and labeling.** Plasmids pDNA (pmaxGFP, Lonza, Switzerland), pLuc (VR1255 Luciferase, Vical, San Diego, CA) and pT7-EGFP-N1 (gift from David Boczkowski, Duke University) were propagated in *Escherichia coli* DH5 $\alpha$  (Invitrogen, Carlsbad, CA) and purified with EndoFree Plasmid Mega and Maxi kits (Qiagen, Germantown, MD). Following linearization, *in vitro* transcription was performed on T7-EGFP-N1 with the mMESASGE mMACHINE T7 kit (Invitrogen) to generate mRNA encoding GFP. To enable attachment of fluorescent labels, pDNA was biotinylated as described by the manufacturer (Label IT Biotin, Mirus Bio, Madison, WI) but scaled to have approximately one to two biotin labels per molecule, then purified from unreacted reagents by ethanol precipitation. Biotinylated samples were reacted with streptavidin-functionalized quantum dots (QDs, Qdot 605 ITK, Invitrogen) as described previously<sup>32</sup>. Nucleic acid was added in excess to QDs to ensure no unreacted QDs remained. The QDs were matched with the Cy5 used to label the polymer to comprise a quantum dot Förster resonance energy transfer (QD-FRET) pair that was used to assess the intracellular binding status of polyplexes.

**Fabrication and operation of microfluidic device.** Cross-flow droplet generators were fabricated using conventional soft lithography<sup>33,34</sup>. PDMS prepolymer was cast and cured on an SU-8 3025 (MicroChem, Newton, MA) master (Transparency mask, CAD/Art Services, Bandon, OR), which produced a channel height of approximately 35  $\mu$ m. PDMS prepolymer (Sylgard 184 Silicone Elastomer Kit, Dow Corning, Midland, MI) was prepared in a 10:1 (base:curing agent) ratio and cured at 65°C for 1 hr. The cured PDMS was then excised, punched with through-holes to accept fluidic connections, and bonded to glass cover slips using a thin layer of spin-coated PDMS to create channels surrounded by PDMS on all sides. The fully assembled chips were then left in an oven at 95°C overnight to promote complete bonding.

Prior to use, the microfluidic channels were flushed with the oil phase solution for 30 minutes to ensure wetting. To generate polyplexes, two syringe pumps (PHD2000, Harvard Apparatus, Holliston, MA) were used to infuse the oil/surfactant mix and aqueous reagents independently through syringe tubing adapters (Hamilton, Reno, NV). The oil phase consisted of FC-40 fluorocarbon oil (3 M, St. Paul, MN) and 2% PEGylated fluorosurfactant (EA Surfactant RainDance Technologies, Lexington, MA or PicoSurf 1, Dolomite Microfluidics, Royston, UK). Flow rates were set at 7.5  $\mu$ L min<sup>-1</sup> for the oil phase input and 2.5  $\mu$ L min<sup>-1</sup> for each of the three aqueous inputs. Water-in-oil droplets (~100 pL) were generated at the channel junction, where the polymer and nucleic acid solutions, separated by a buffer channel, were introduced to the continuous oil phase. Polyplexes self-assembled while confined to the droplets, while mixing of their components was enhanced by the inclusion of a serpentine channel segment<sup>35</sup>. MAC polyplexes were collected by breaking the droplets (Droplet Destabilizer, RainDance Technologies) and used directly from the aqueous supernatant for subsequent characterization or cellular investigation without any further purification. Bulk preparation was performed following published protocols<sup>31</sup>. Briefly, polyplexes were prepared by adding a complexation buffer solution (20 mM HEPES, 5 wt% glucose, pH 7.4) of polymer (844  $\mu$ g mL<sup>-1</sup> for DNA, 1125  $\mu$ g mL<sup>-1</sup> for RNA) to a complexation buffer solution of nucleic acid (75  $\mu$ g mL<sup>-1</sup>) followed immediately by 20 seconds of vortex mixing. Reaction sizes ranged from 5 to 15  $\mu$ g of nucleic acid. The presence of the reagents used for MAC droplet generation did not significantly affect the activity of bulk products (Supplementary Figure 3). Identical reagent solutions and concentrations were introduced into the droplet generator to produce MAC polyplexes.

**Nanocomplex characterization.** Polyplex sizes and zeta potentials were measured with a Zetasizer NanoZS-90 (Malvern Instruments, Southborough, MA). Polyplexes were assayed at a nucleic acid concentration of 15  $\mu$ g mL<sup>-1</sup> for size measurements. Measurements of five independent samples were performed at 25°C using a 90° scattering angle. To assess aggregation kinetics, measurements were repeated at five-minute intervals over a four-hour period. Size is reported as the Z-average diameter, or intensity weighted mean hydrodynamic diameter. Zeta-potential measurements were performed on five independent samples at a final DNA concentration of 3  $\mu$ g mL<sup>-1</sup> using a capillary flow cells (Malvern Instruments) in complexation buffer at pH 7.4 and 25°C.

**Cell culture and transfection.** For all cell culture experiments, 20,000 cells cm<sup>-2</sup> cells were seeded 24 hours prior to transfection in 24-well TCPS plates (BD, Franklin Lakes, NJ) and cultured at 37°C and 5% CO<sub>2</sub> in the appropriate complete growth media recommended by the supplier. The cell types studied were human embryonic kidney HEK293 (ATCC, Manassas, VA), human hepatocellular carcinoma HepG2 (ATCC), primary mouse embryonic fibroblasts (PMEF) (Millipore, Manassas, VA), and human mesenchymal stem cells (hMSC) (ATCC). All transfections were carried out at 37°C and 5% CO<sub>2</sub> in serum- and antibiotic-free OptiMEM (Invitrogen), which was replaced with the appropriate complete growth medium 4 hours after the onset of transfection. Each transfection was performed in duplicate and quantified results represent three independent experiments. Transfection efficiency and transgene expression were assayed at 24 hours post-transfection. Luminescence measurements to quantify luciferase expression were performed using the SteadyGlo kit (Promega, Madison, WI) according to the manufacturer's protocol.

**Flow cytometry.** Flow cytometric analysis was performed using a FACSCanto II (BD Biosciences, Franklin Lakes, NJ) with at least 10,000 cells analyzed per sample. To quantify transfection efficiency 24 hours after transfection, cells were washed briefly with PBS without Ca<sup>2+</sup> and Mg<sup>2+</sup> (Mediatech, Washington, DC), and released from TCPS surfaces with 0.25% Trypsin-EDTA (Invitrogen). The trypsin was inactivated with serum-containing media and the cells were centrifuged at 4°C, resuspended in ice-cold PBS, centrifuged again, and resuspended in PBS containing 1% paraformaldehyde (PFA) (EMS, Hatfield, PA). The FSC/SSC was gated with untreated cells to exclude the dead cells or cell debris. Cells transfected with non-fluorescent pLuc plasmid served as negative controls for each equivalent pDNA or mRNA dose, with gating such that 1% of these cells were considered GFP<sup>+</sup>.

Cellular uptake of polyplexes was evaluated in separate experiments using unlabeled p(CBA-ABOL) polymer and QD-labeled pDNA. After predetermined post-transfection incubation periods at 37°C, cells were washed briefly with PBS without Ca<sup>2+</sup> and Mg<sup>2+</sup> and released from TCPS surfaces with 0.25% Trypsin-EDTA. The trypsin was inactivated with serum-containing media and the cells were centrifuged at 4°C, resuspended in ice-cold PBS, centrifuged again, and resuspended in PBS containing 4% PFA and 2% glutaraldehyde for 15 minutes. The cells were washed with PBS, washed again with PBS containing heparin in PBS (20 units mL<sup>-1</sup>) to remove membrane bound complexes, and then resuspended in PBS for analysis<sup>36</sup>. Timepoints represent the elapsed time from the start of transfection until the onset of trypsinization. The 405 nm laser served as the excitation source and the fluorescence emission was captured using the P10 channel (dichroic: 502 LP, emission filter: 622/36 nm). To measure rates of intracellular unpacking, cells were transfected using 1:4 Cy5-labeled to unlabeled polymer complexed with QD-labeled pDNA. Samples were prepared using the same procedure described for the cellular uptake studies, however time zero was defined instead as the change from transfection medium back to growth medium for unpacking analyses. We examined the decay of the QD-FRET emission signal over time. Detection was accomplished by excitation with the 405 nm laser and 650 LP emission filter. The fluorescence signals were compensated and gated with negative and single-color controls. FlowJo (v. 9.1, Tree Star, Ashland) and FACSDiva (BD) were used to analyze the results.

**Fluorescence microscopy.** Epifluorescent images were captured with an inverted fluorescence microscope (TE2000U, Nikon Instruments, Melville, NY) equipped with a 100-W mercury arc lamp (X-Cite 120 Fluor system, EXFO, Ontario, Canada) and a cooled CCD (CoolSnap HQ, Roper Scientific, Tucson, AZ). Monochromator emission from GFP was collected and filtered through appropriate filters and dichroics. Image processing and analysis was performed with ImageJ (v1.43, <http://rsb.info.nih.gov/ij/>).

**Nanocomplex stability and free polymer measurements.** Titrated volumes PicoGreen or RiboGreen (Quant-iT, Invitrogen) reagent were added to polyplex solutions in a 96-well plate and incubated for 15 minutes before measuring the signal using a plate reader (BMG Labtech GmbH, Germany). To plot polyplex stability, the background fluorescence was subtracted and the measured fluorescence intensity as normalized to the signal in control samples containing no polymer. To quantify the amount of unreacted polymer remaining in solution following polyplex preparation, 10  $\mu$ g of polyplexes were prepared using 4:1 p(CBA-ABOL) to Cy5-labeled p(CBA-ABOL90/BDA10) and centrifuged at 14,000  $\times$  g for 30 minutes to remove the particulate fraction. The supernatant was then collected, lyophilized then resuspended in 100  $\mu$ L complexation buffer. The suspensions were added to a 96-well plate and the Cy5 signal was quantified. Following subtraction of the background signal, the percentage of free polymer remaining was determined by a standard curve constructed with titrated polymer solutions.



**Statistical analysis.** Results are reported as the mean  $\pm$  S.E.M. as described for three or more independently performed experiments. Asterisks denote p-values  $< 0.05$ . Statistical significance was determined using an unpaired t-test (Prism 5.0, GraphPad Software, La Jolla, CA). Two-tailed p-values are reported unless otherwise stated.

- Shigematsu, H. *et al.* Randomized, double-blind, placebo-controlled clinical trial of hepatocyte growth factor plasmid for critical limb ischemia. *Gene Ther* **17**, 1152–1161 (2010).
- Nathwani, A. C. *et al.* Adenovirus-associated virus vector-mediated gene transfer in hemophilia B. *N Engl J Med* **365**, 2357–2365 (2011).
- Morishita, R. *et al.* Phase I/IIa clinical trial of therapeutic angiogenesis using hepatocyte growth factor gene transfer to treat critical limb ischemia. *Arterioscler Thromb Vasc Biol* **31**, 713–720 (2011).
- Bennett, J. *et al.* AAV2 gene therapy readministration in three adults with congenital blindness. *Sci Transl Med* **4**, 120ra115 (2012).
- Davis, M. E. *et al.* Evidence of RNAi in humans from systemically administered siRNA via targeted nanoparticles. *Nature* **464**, 1067–1070 (2010).
- Tang, B. C. *et al.* Biodegradable polymer nanoparticles that rapidly penetrate the human mucus barrier. *Proc Natl Acad Sci U S A* **106**, 19268–19273 (2009).
- Lai, S. K., Wang, Y. Y. & Hanes, J. Mucus-penetrating nanoparticles for drug and gene delivery to mucosal tissues. *Adv Drug Deliv Rev* **61**, 158–171 (2009).
- Fernandez, C. A. *et al.* Metabolically stabilized long-circulating PEGylated polyacridine peptide polyplexes mediate hydrodynamically stimulated gene expression in liver. *Gene Ther* **18**, 23–37 (2011).
- Chen, J., Wu, C. & Oupicky, D. Bioreducible hyperbranched poly(amido amine)s for gene delivery. *Biomacromolecules* **10**, 2921–2927 (2009).
- Pack, D. W., Hoffman, A. S., Pun, S. & Stayton, P. S. Design and development of polymers for gene delivery. *Nat Rev Drug Discov* **4**, 581–593 (2005).
- Grigsby, C. L. & Leong, K. W. Balancing protection and release of DNA: tools to address a bottleneck of non-viral gene delivery. *J R Soc Interface* **7 Suppl 1**, S67–82 (2010).
- Braun, C. S. *et al.* A stopped-flow kinetic study of the assembly of nonviral gene delivery complexes. *Biophys J* **88**, 4146–4158 (2005).
- Ho, Y. P., Chen, H. H., Leong, K. W. & Wang, T. H. The convergence of quantum-dot-mediated fluorescence resonance energy transfer and microfluidics for monitoring DNA polyplex self-assembly in real time. *Nanotechnology* **20**, 095103 (2009).
- Fant, K., Norden, B. & Lincoln, P. Using ethidium to probe nonequilibrium states of DNA condensed for gene delivery. *Biochemistry* **50**, 1125–1127 (2011).
- Rolland, J. P. *et al.* Direct fabrication and harvesting of monodisperse, shape-specific nanobiomaterials. *J Am Chem Soc* **127**, 10096–10100 (2005).
- Tao, L., Zhao, X. M., Gao, J. M. & Hu, W. Lithographically defined uniform worm-shaped polymeric nanoparticles. *Nanotechnology* **21**, 095301 (2010).
- Kim, J. *et al.* Microfluidic approaches for gene delivery and gene therapy. *Lab Chip* **11**, 3941–3948 (2011).
- Koh, C. G. *et al.* Delivery of polyethylenimine/DNA complexes assembled in a microfluidics device. *Mol Pharm* **6**, 1333–1342 (2009).
- Debus, H., Beck-Broichsitter, M. & Kissel, T. Optimized preparation of pDNA/poly(ethylene imine) polyplexes using a microfluidic system. *Lab Chip* **12**, 2498–2506 (2012).
- Koh, C. G. *et al.* Delivery of antisense oligodeoxyribonucleotide lipopolyplex nanoparticles assembled by microfluidic hydrodynamic focusing. *J Control Release* **141**, 62–69 (2010).
- Hsieh, A. T. *et al.* Nonviral gene vector formation in monodispersed picoliter incubator for consistent gene delivery. *Lab Chip* **9**, 2638–2643 (2009).
- Ho, Y. P., Grigsby, C. L., Zhao, F. & Leong, K. W. Tuning physical properties of nanocomplexes through microfluidics-assisted confinement. *Nano Lett* **11**, 2178–2182 (2011).
- Gary, D. J., Puri, N. & Won, Y. Y. Polymer-based siRNA delivery: perspectives on the fundamental and phenomenological distinctions from polymer-based DNA delivery. *J Control Release* **121**, 64–73 (2007).
- Martens, T. F. *et al.* Measuring the intravitreal mobility of nanomedicines with single-particle tracking microscopy. *Nanomedicine (Lond)* (2013).
- Adler, A. F. *et al.* Nonviral direct conversion of primary mouse embryonic fibroblasts to neuronal cells. *Mol Ther Nucleic Acids* **1**, e32 (2012).
- Wang, Y., Zhang, L., Wang, Q. & Zhang, D. Stability issue of nanosuspensions in drug delivery. *J Control Release*, Advance online publication (2013).
- Fischer, D., Li, Y., Ahlemeyer, B., Krieglstein, J. & Kissel, T. In vitro cytotoxicity testing of polycations: influence of polymer structure on cell viability and hemolysis. *Biomaterials* **24**, 1121–1131 (2003).
- Chen, H. H. *et al.* Quantitative comparison of intracellular unpacking kinetics of polyplexes by a model constructed from quantum dot-FRET. *Mol Ther* **16**, 324–332 (2008).
- Zauner, W., Farrow, N. A. & Haines, A. M. In vitro uptake of polystyrene microspheres: effect of particle size, cell line and cell density. *J Control Release* **71**, 39–51 (2001).
- Grigsby, C. L., Ho, Y. P. & Leong, K. W. Understanding nonviral nucleic acid delivery with quantum dot-FRET nanosensors. *Nanomedicine (Lond)* **7**, 565–577 (2012).
- Lin, C. *et al.* Novel bioreducible poly(amido amine)s for highly efficient gene delivery. *Bioconjug Chem* **18**, 138–145 (2007).
- Ho, Y. P., Chen, H. H., Leong, K. W. & Wang, T. H. Evaluating the intracellular stability and unpacking of DNA nanocomplexes by quantum dots-FRET. *J Control Release* **116**, 83–89 (2006).
- Qin, D., Xia, Y. & Whitesides, G. M. Soft lithography for micro- and nanoscale patterning. *Nat Protoc* **5**, 491–502 (2010).
- Song, H., Chen, D. L. & Ismagilov, R. F. Reactions in droplets in microfluidic channels. *Angew Chem Int Ed Engl* **45**, 7336–7356 (2006).
- DeMello, A. J. Control and detection of chemical reactions in microfluidic systems. *Nature* **442**, 394–402 (2006).
- Khalil, I. A., Kogure, K., Futaki, S. & Harashima, H. High density of octaarginine stimulates macropinocytosis leading to efficient intracellular trafficking for gene expression. *J Biol Chem* **281**, 3544–3551 (2006).

## Acknowledgments

This work is supported by NIH (EB015300 and AI096305), NSF EEC-0425626, Lundbeck Foundation (R95-A10275 to YPH), and a predoctoral fellowship from the American Heart Association (C.L.G.). We thank Dr. Mike Cook and the Flow Cytometry Shared Resource at the Duke Cancer Institute for their support. We also thank David Boczkowski (Duke University) for supplying the pT7-EGFP-N1 construct and RainDance Technologies for providing the EA Surfactant and Droplet Destabilizer.

## Author contributions

C.G. and Y.H. conceived and designed the study, performed experiments, assembled, analyzed and interpreted data and helped write the manuscript; C.L. provided materials and helped write the manuscript. J.E. and K.L. conceived and designed the study, analyzed and interpreted data, and helped write the manuscript.

## Additional information

Supplementary information accompanies this paper at <http://www.nature.com/scientificreports>

**Competing financial interests:** The authors declare no competing financial interests.

**How to cite this article:** Grigsby, C.L., Ho, Y.-P., Lin, C., Engbersen, J.F.J. & Leong, K.W. Microfluidic Preparation of Polymer-Nucleic Acid Nanocomplexes Improves Nonviral Gene Transfer. *Sci. Rep.* **3**, 3155; DOI:10.1038/srep03155 (2013).



This work is licensed under a Creative Commons Attribution-NonCommercial-NoDerivs 3.0 Unported license. To view a copy of this license, visit <http://creativecommons.org/licenses/by-nc-nd/3.0>